

Design considerations and performance of a combined scanning tunneling and scanning electron microscope

A. Wiessner^{a)} and J. Kirschner

Max-Planck-Institut für Mikrostrukturphysik, Weinberg 2, D-06120 Halle, Saale, Germany

G. Schäfer and Th. Berghaus

OMICRON, Vakuumphysik GmbH, Idsteiner Strasse 78, D-65232 Taunusstein, Germany

(Received 11 March 1997; accepted for publication 25 June 1997)

We designed and built a combination of a scanning tunneling microscope (STM) and a scanning electron microscope (SEM) which is working under ultrahigh vacuum conditions (base pressure typically $7 \cdot 10^{-11}$ mbar). The SEM is ideally used for surveying the sample and to control the STM tip positioning, while the STM extends the resolution range into the atomic scale. The design concept allows moving the STM tip freely over the sample under SEM control and using both imaging techniques simultaneously. The system is equipped with an electron energy analyzer (cylindrical sector analyzer) providing Auger electron spectroscopy, scanning Auger microscopy (SAM) and x-ray photoelectron spectroscopy capabilities. In addition, low energy electron diffraction and reflection high energy electron diffraction facilities are installed. In order to use these very different imaging techniques *in situ*, several special solutions had to be incorporated in the design of the system; they are described in detail. Some results are presented which demonstrate the performance of the STM/SEM system. Atomic resolution of the STM, a SEM resolution of up to 20 nm, and a SAM resolution of better than 100 nm were achieved. © 1997 American Institute of Physics. [S0034-6748(97)04409-2]

I. INTRODUCTION

Two techniques are mainly used in surface science to image structures on a nanometer scale: scanning electron microscopy (SEM) and scanning tunneling microscopy (STM).^{1,2} Both imaging techniques have their well known advantages and disadvantages. The SEM can do fast imaging of large sample areas, allowing easy location of interesting features by quickly zooming in and out at various sample positions. The large depth of field makes the image interpretation easy. However, there is no resolution in normal direction and the lateral resolution is generally limited by electron-optical restrictions. The STM has ultimate z resolution of about 0.01 nm and achieves a lateral resolution down to the atomic scale. It includes the feasibility of local electron spectroscopy of electronic states, and nanostructuring. But the STM's way of piezomechanically moving a tip in nanometer distance across the sample surface results in a very slow scan speed and limits the field of view to typically some micrometers. In addition, the coarse approach of the tip into tunneling mode is a sensitive process which has to be performed carefully to avoid a tip crash. This makes the examination of large sample areas impractical. Particularly, if it is necessary to investigate areas spread all over the sample or far apart from each other, it is tedious and time consuming to find them and to get a representative overview. An example for such a sample is given in Sec. IV. Samples with small, localized features of interest, for example interfaces or superlattices in semiconductors, are extremely difficult to study in conventional STM. These regions can hardly be approached reproducibly without the use of the SEM assisting in the tip positioning. With the *in situ* combination

of STM and SEM both imaging techniques are ideally complementing. The SEM is used to search for the area of interest for further STM examination. The STM tip is then guided to the selected area and precisely positioned at a structural detail, all under SEM control. Switching to STM now offers subnanometer resolution capability. In the SEM image also the quality of the STM tip can be checked. For samples which are sensitive to contamination, both imaging techniques have to be operated under ultra high vacuum (UHV) conditions (pressure below $1 \cdot 10^{-10}$ mbar). Otherwise the electron beam of the SEM will crack adsorbed molecules, especially hydrocarbons³⁻⁵ which form a contamination layer on the sample. For the STM such a layer will largely reduce the resolution power and even prohibit imaging the true surface. Also the AES and SAM performance will be largely reduced since the surface exit depth of the Auger electrons is very small.

In Sec. II we will describe the design considerations for each part of the system, followed by its realization. In Sec. III the performance of the apparatus is discussed. An example for the application of the system is given in Sec. IV.

II. DESIGN CONCEPT AND ITS REALIZATION

A. General design

Several setups have been described which combine an STM with an SEM.³⁻²⁰ All of them are standard SEM systems where the STM part was designed and added later. Our

^{a)}Electronic mail: awiessn@mpi-halle.mpg.de

aim was to design and to build a high performance system combining STM, SEM, and SAM, and optional low energy electron diffraction LEED, reflection high energy electron diffraction RHEED, and x-ray photoelectron spectroscopy XPS. Therefore the major parts of the system, the combined STM/SEM goniometer stage and the analysis chamber had to be designed in parallel.

The combination of an SEM and an STM is a unique instrument if the magnification ranges, or scan areas, of both imaging techniques overlap significantly. In this case the STM extends the resolution down to the atomic scale. Very high resolution of the SEM, better than several tens of nanometers, is no longer necessary. The concept of our design was the following: The SEM magnification should range from $1 \cdot 10^2 \times$ (scan area 1.5×1.5 mm) up to $1 \cdot 10^5 \times$ (scan area $1.5 \times 1.5 \mu\text{m}$). In the same notation the STM will offer a range from $1.5 \cdot 10^4 \times$ (scan area $10 \times 10 \mu\text{m}$) up to approximately $1 \cdot 10^7 \times$ (scan area 15×15 nm). The magnification overlap of one order of magnitude is sufficient for precisely monitoring the tip positioning. In SEM imaging the secondary electron yield depends on the tilt angle of the sample surface. The enhanced emission at edges of structural details increases the topographical contrast. To make use of this effect the sample stage has to be mounted on a goniometer providing variable tilt angles in the range of typically $\pm 45^\circ$ with respect to the electron beam. By this also the angle under which the STM tip is visible in the SEM image can be easily varied. The STM tip should be already visible with the SEM at moderate tilt angles, $\sim 15^\circ - 20^\circ$, in order to achieve SEM imaging with minimum distortion in the x direction. While STM, SEM, and SAM should work simultaneously, LEED, RHEED, and XPS should be applicable without transferring the sample. It was therefore necessary to use a single chamber for all analysis equipment. The necessary angle of movement is then given by the orientation of the analysis tools. If a horizontal sample surface is defined as 0° , then the position of the LEED and the Auger system require a maximum tilt angle of the goniometer stage of -95° and $+40^\circ$, respectively. The optional XPS port which is situated below the Auger system (not shown in Fig. 1) extends this range to $+90^\circ$, therefore we need a goniometer with a total tilt range of 185° (see Fig. 1). Within this range a position is included for convenient exchange of sample plates and of STM tips.

B. Sample and STM stage

1. Design considerations

For SEM and STM operation without mutual restrictions the sample and the scanner tip have to be independently movable with respect to the SEM's field of view. This requires individual x, y, z translations for both the sample stage and the STM scanner, and a rotational movement of the combined setup for performing the angular tilt motion. With the STM's z movement the scanner tip is approached into tunneling contact. The z movement of the sample holder is necessary to achieve tilt eucentricity for samples of different thicknesses. In addition, the electron-optical axis also has to be prealigned with the goniometer axis. For this the electron

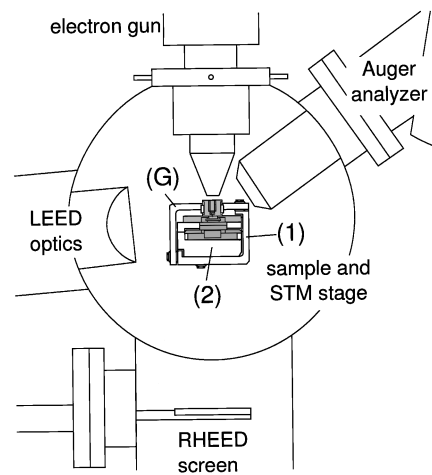


FIG. 1. Schematic drawing of the analysis chamber (front view). The goniometer STM/SEM stage is mounted in the center of the chamber and the analysis equipment is placed on a circle around the sample holder. (G) denotes the goniometer, (1) the first and (2) the second stage of the viton stack damping system.

column has to be mounted on an x, y translational stage. When the tilt eucentricity is established the SEM or SAM image will not shift significantly when the tilt angle is changed. Therefore, the necessary precision of the eucentricity is given by the field of view of the SEM at intermediate magnifications and the maximum available electron-optical image shift of the SEM at large magnifications. An accuracy of better than $100 \mu\text{m}$ seems desirable and practicable.

Only the combination of translational and rotational degrees of freedom described above enables one to investigate each region on the sample freely by SEM and STM. All translational motions should be driven by motors which are free from backlash, fully UHV compatible and sufficiently stable for STM measurements. A good choice are piezo inertia drives. These motors allow a very compact design, and do not induce vibration.

Combining an SEM with an STM is difficult, since the requirements on the vibration damping are opposite. The working distance of an STM is only a few nanometers, an excellent position stability of the sample with respect to the scanner tip is therefore imperative. This is only fulfilled if the STM is decoupled from vibration of the chamber. Usually the sample holder/STM assembly is spring suspended with an eddy-current damping. On the other hand, the SEM operation requires a stiff mounting of the sample with respect to the electron column. Combining both imaging techniques therefore requires a careful design of the damping system: the combined sample and STM stage has to be mounted on the goniometer via an internal damping (see Fig. 2). We considered a two-stage Viton damping with the center of gravity coinciding with the center of mounting to give the highest performance. As this mounting will reduce the high frequency vibration only, the low frequency vibration has to be reduced by setting the whole UHV system onto a vibration isolating support.

2. Realization

For the sample stage three independent combinations of piezo inertia drives, based on the OMICRON micro piezo

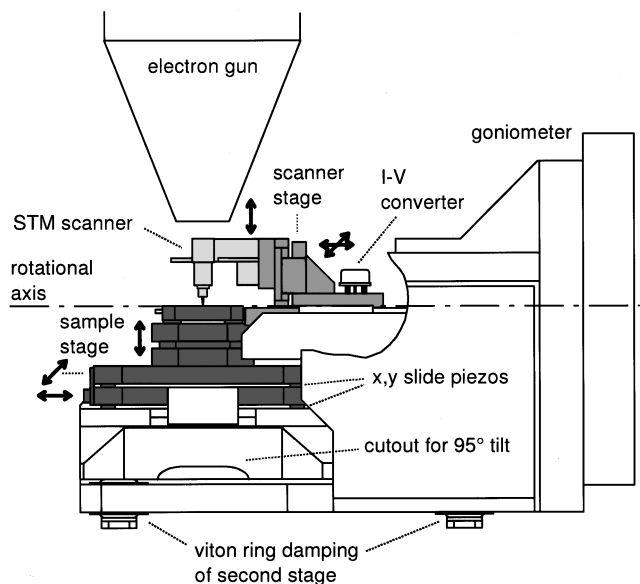


FIG. 2. Design of the sample and STM scanner stage (side view). The sample holder is shown in dark gray, the STM stage in medium gray and the removable part of the STM (scanner head) in light gray, the goniometer is not shadowed. The $I-V$ converter IC is placed on the STM stage. The rotation axis is marked with a dashed line.

slides, perform the x, y, z movements (see Fig. 2, the sample table is marked in dark gray). The piezo motor uses slip/stick effects related to inertia forces when a piezo is driven in a fast/slow sequence. A sawtooth voltage with an amplitude of ± 80 V to ± 400 V is applied to the piezos, corresponding to a step width of 20–400 nm. The sliders are transported during the slow shear movement of the piezos and remain immobile due to their inert mass while the piezos slip during the fast rebound motion. The mobile and the immobile part of these sliders are held together by magnetic forces rather than gravity, which ensures independence of orientation. This is especially important for the LEED, RHEED, and XPS geometries, where the stage is tilted $\pm 90^\circ$ and the x, y micro piezo drives work against gravity.

Sample movement is realized by a stack of three linear translation micro piezo slides, with travels of 10 mm in x and y directions and 5 mm in the z direction. The design of the STM scanner stage is slightly different. A combination of three shear piezos allows the coarse positioning of the STM in the x, y plane (see Fig. 2, the STM table is marked in medium gray). Only the movement in y direction is a translation, in x direction it is a rotation around the rear piezo, which is guided by a V groove. For the y movement it offers a range of 12 mm, in the x direction 5 mm. The large y range is necessary to remove the scanner entirely from the scan area of the SEM and SAM. For the z movement of the scanner (5 mm range) the same piezo drives are used. Only the tilt movement was realized by a mechanical bearing stage (Raith Precision Goniometer Stage²¹) which was slightly modified for full UHV compatibility, for example by adding gas relief holes for all trapped volumes and cleaning to UHV standards. This goniometer has originally been designed for high resolution SEM imaging, a rotational range of 360° and a gear ratio of 1° at the goniometer bearing per turn at the

rotational feedthrough. The tilt angle is reproducible with an accuracy of 1° .

The sample holder is electrically isolated from its support for applying the gap voltage for STM measurements. Also taking a sample current image with the SEM is then possible.

The damping system incorporates two stages which are perpendicular to each other. As pointed out in the design considerations the center of gravity coincides with the center of mounting, independent of the tilt angle of the goniometer. Both stages are assembled via three screws isolated with several viton rings each. This relatively bulky setup requires some cutouts to avoid interference with other equipment at large tilt angles.

C. STM system

1. Design considerations

In our design the STM scanner head must fit between the electron column and the sample with the goniometer in normal and tilted position. Nevertheless, the working distance of the column should be as small as possible to maintain the SEM image resolution. The scanner tube should be of small diameter to offer tip visibility with the SEM at small tilt angles. For scanner designs using thicker tubes the tip has to be mounted out of center, otherwise the tube will shadow the tip. In our design the minimum tilt angle should not exceed 30° for obtaining only small SEM image distortion. Furthermore, if performing SEM and STM measurements simultaneously one has to ensure that the voltages applied to the piezo tube will not distort the SEM image. The tube therefore has to be electrostatically shielded which increases, however, the outer diameter of the scanner. The whole scanner head has to be removable from its support for two reasons: First, for quick tip replacement it has to be taken out of the vacuum system. Second, if mounted the scanner will shadow the LEED pattern for large diffraction angles.

2. Realization

The exchangeable STM scanner head is held to the stage by a magnet, the exact position is obtained by guiding it with two pins (see Fig. 2, the STM scanner head is marked in light gray). The guide pins are used to center the scanner correctly with respect to the electrical contacts at the stage, they are not meant to accomplish any further positioning of the STM tip with respect to a sample region. The stray field of the magnet is shielded with the scanner head both at the STM and the carousel reception. The electrical contact to the tip and the scanner piezo tube is obtained by eight spring loaded pins. To achieve optimum signal to noise ratio the current to voltage ($I-V$) converter is placed directly behind the scanner head inside the vacuum system (see Fig. 2). To reduce the influence of stray electromagnetic fields most of the electrical wires to the stage and the scanner head are either in twisted pair configuration or shielded.

The scanner head currently used is based on a 1/8-in.-thick, 1/2-in.-long piezo tube with a wall thickness of 0.5 mm. With a maximum operation voltage of ± 140 V this

scanner achieves a field of view of about $10 \times 10 \mu\text{m}$. With this scanner the tip is mounted in-center and fixed with a small screw. The piezo tube is shielded to avoid shifts of the SEM image due to the large voltages applied to the piezo electrodes.

The tip coarse approach can be monitored with a charge coupled device (CCD) camera which is mounted to a chamber viewport. The distance of the tip to the sample can be estimated by the relative positions of the tip and its mirror image on the sample. The OMICRON SCALA system, incorporating a SUN compatible workstation and a scanning probe method (SPM) control unit, handles the whole measurement process. The workstation allows data acquisition and image processing simultaneously.

D. SEM system

1. Design considerations

As pointed out in Sec. II A, ultrahigh resolution of the SEM system is not necessary since the STM will extend the resolution range down to the sub-nm scale. This consideration offers using a compact electron gun with a resolution limit of several tens of nanometers. Important considerations for the choice of the electron gun are: the gun must work under UHV condition, it should offer a large working distance of about 25 mm, and finally, high beam currents should be available since the electron gun is to be used also for Auger measurements. As described in Sec. II B the electron optical axis has to be aligned with the goniometer axis for achieving tilt eucentricity of the sample stage.

2. Realization

We use a UHV compatible, fully electrostatic electron gun (FEI Stacked Disk Double Lens Electron Column²²) which operates with a Schottky emitter. The beam energy ranges from 1 kV up to 25 kV. A beam current up to 200 nA can be achieved. The resolution limit is 20 nm at a beam energy of 25 kV. Attached to the gun is a small ion getter pump and the column can be isolated from the analysis chamber by a gate valve. For the required adjustment of the electron column we designed a stiff and rigid translational stage, which can be moved 3 mm vectorial from the center (see Fig. 1). This movement is done by a set of four micrometer screws acting on the insertion plate which carries the flange with the electron gun.

The electron beam is focused by a two stage electrostatic lens system with beam defining aperture between the lenses. During adjustment and for selection of the beam current the beam is deflected by a blanking electrode to an aperture and the current is measured with a picoammeter. The secondary electrons are detected by means of an electron multiplier with a bias grid [secondary electron detector (SED)], the signal is amplified and finally digitized on a PC interface card. An IBM compatible PC and the Spectra software V6²³ are used to control the scan and data acquisition. The images are displayed in 256 gray levels, 200×200 pixel resolution with a refresh rate of about 3 Hz on a i486DX33 or about 10 Hz on a Pentium 100 based system. A video option allows

the display of realtime images with TV rate on a video monitor. For image capturing, several slow scan modes are available which improve the signal to noise ratio.

E. Auger electron spectroscopy and SAM

1. Design considerations

The large beam current of the electron gun allows the acquisition of AES and performing SAM. The operation with the STM/SEM combination prevents the use of a standard cylindrical mirror analyzer (CMA). Such a CMA normally has a small working distance typically in the range of 10–30 mm, which would interfere with the SEM and the STM setup. Either a very compact CMA or an analyzer with transfer optics has to be used.

2. Realization

As electron energy analyzer we use a cylindrical sector analyzer (FOCUS CSA 300²⁴) (see Fig. 1). Since it operates with a transfer optics, it offers a large working distance of about 50 mm, which fits our requirements. The electrons are detected with an electron multiplier, and the pulses are counted on a PC interface card. Similar to SEM the Spectra software controls the Auger measurements. Standard Auger spectra can be measured up to 3.2 keV. The acceptance area of the CSA is large enough, about 3 mm in diameter, so an adjustment with respect to the primary beam is of less importance.

F. Additional analysis tools

1. Design considerations

Although the magnification of the system ranges from optically visible down to the atomic scale, information about the crystal structure of the samples is not available with STM, SEM, and Auger measurements. Other analysis techniques have to be used for obtaining such information. We chose to use both RHEED and LEED. With a RHEED system it is possible to scan the crystal structure of the sample, the LEED offers measuring it with high precision. Furthermore, flanges should be reserved for mounting additional equipment: an x-ray source, an ion gun, and evaporators.

2. Realization

RHEED: A phosphorous screen is used to monitor the RHEED pattern. It is mounted on a holder in the lower part of the analysis chamber (see Fig. 1) and is movable in the x, y plane. The electron gun of the SEM is also used for the RHEED system. Therefore small spot analysis with high resolution is possible and within the limitation imposed by the large tilt angles the correlation between the SEM image and the RHEED pattern can be investigated. The intensity of a selected spot is measured with an electron multiplier, placed behind an aperture in the screen. This aperture is variable to adjust the lateral resolution and the intensity.

LEED optics: The analysis chamber is equipped with a 4-grid rear-view LEED optics with an independent integral electron source (OMICRON SPECTALEED, see Fig. 1). This optics offers performing standard LEED measurements

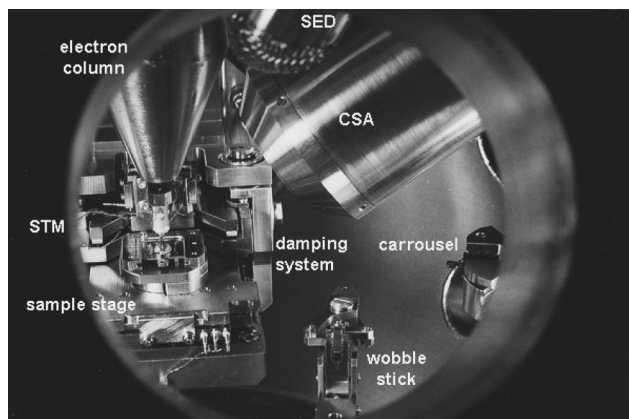


FIG. 3. View inside the analysis chamber.

and retarding field Auger electron spectroscopy. Since the STM scanner head is removable, shadowing of the LEED pattern at large diffraction angles is avoided. The LEED optics can be retracted to allow for full tilt of the goniometer. The goniometer stage can be tilted fully towards the LEED optics without collision between sample stage and electron gun. Of the images shown here, this is best visible in Fig. 3 (front view) and Fig. 2 (side view).

G. UHV chamber system

1. Design considerations

It is good UHV practice to have a preparation chamber separated from the analysis chamber. In this case samples can be prepared without affecting the pressure of the analysis chamber. A third chamber is necessary: for sample and scanner head exchange the UHV system should incorporate an entry lock. This chamber should be linked to the preparation chamber for again preserving a good vacuum inside the analysis chamber during a transfer cycle.

As described in the design considerations of the sample and STM stage (see Sec. II B), the whole chamber system should be isolated from ground vibrations.

2. Realization

For stability reasons all chambers are mounted to a rigid bench with additional support for heavy or large extending items. The analysis chamber is made from thick walled stainless steel with reinforced structure. A gate valve separates analysis and preparation chamber. The fast entry lock is connected to the preparation chamber by a valve. All analysis equipment described in the previous sections is fitted to the analysis chamber Fig. 4. Samples can be stored in a 6-slot carousel of which two slots can also be used for STM scanner heads. The transfer of samples between the carousel and the stage is conveniently carried out with a wobble stick, which is also used for placing the scanner head to the STM stage. Samples and the STM scanner heads can be exchanged via the preparation chamber and the fast entry lock using magnetically coupled linear/rotary motion devices. A port is fitted to the fast entry lock which enables mounting a transportable vacuum chamber. This chamber allows transferring samples under UHV conditions between several systems in

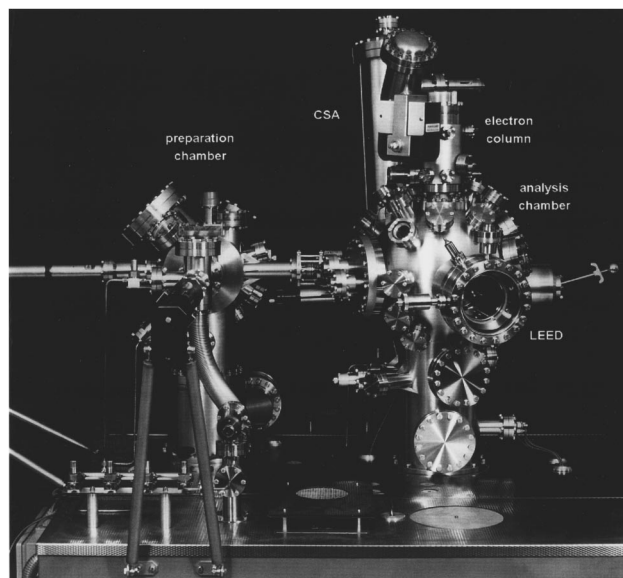


FIG. 4. The complete STM/SEM system.

our institute. All equipment necessary for sample preparation is mounted to the preparation chamber, currently equipped with an ion sputter gun and two evaporators. Both resistor (radiation) heating up to a temperature of 900 °C and direct sample heating are possible on the manipulator of this chamber.

The two chambers are separately pumped by ion getter pumps and titanium sublimation pumps (TSP). A base pressure of typically $7 \cdot 10^{-11}$ mbar is reached. Operation of the electron gun does not affect the vacuum. A turbo molecular pump (TMP) is connected to the preparation chamber. It is used for pumping during system bake-out and sputtering. The analysis chamber is prepared for mounting an additional TMP. A second TMP is used to evacuate the fast entry lock and the gas inlet system, and for differential pumping of the ion gun. After a transfer cycle or after sputtering the base pressure is restored within several minutes. The whole UHV chamber system is mounted on a rigid bench resting on four pneumatic vibration isolating legs (IDE²⁵).

III. PERFORMANCE

A. SEM

The magnification of the SEM was calibrated using a checkerboard pattern sample with squares of four different sizes from 1×1 mm down to 1×1 μ m. An aluminum-tungsten dendrite test sample was used to check the resolution of the SEM. Structures, for example spaces between dendritic fingers, in the range of < 50 nm, typically 20 nm, are resolved. The SEM performance reaches the resolution limit of the electron column; no mechanical vibration is visible. This result shows that our arrangement of an internal and an external damping system is appropriate for the SEM resolution needed.

The influence of the STM on the SEM image is negligible. When reversing the voltage applied to the scanner electrodes, which can be up to 150 V, the SEM image shifts only slightly, less than 1 μ m. However, the intensity of the

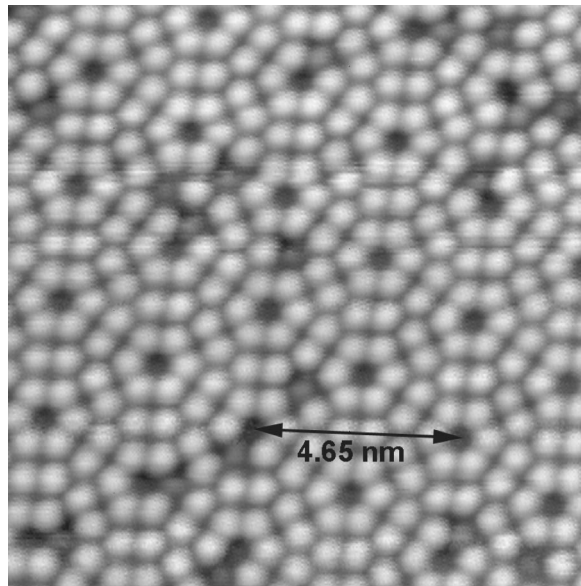


FIG. 5. Atomic resolution of the apparatus, demonstrated on Si(111)7×7. The sample was prepared according to Ref. 26. The image is neither drift compensated nor image processed.

image is reduced due to the scanner assembly shadowing the secondary electrons. A similar shadowing effect can be used to estimate the distance of the tip to the sample: when using mainly backscattered electrons for imaging by changing the bias voltage on the electron multiplier from positive to about -50 V, their pathway from the sample to the detector is more or less linear. The area hidden by the tip then appears as a dark area on the sample.

B. STM

The checkerboard sample was also used for checking the scan area and large scale calibration of the STM scanner. In the SEM image it is easy to observe the tip moving relative to the squares of the sample. The squares give a direct measure of the movement area. As expected the displacement becomes slightly nonlinear for large displacements. Standard test measurements on a Si(111)7×7 sample were performed to check the resolution of the STM system. The sample was prepared according to Ref. 26. Atomic resolution of the STM was obtained, as shown in Fig. 5. Thus, the combined damping system is well adequate also for high STM resolution.

C. Influence of the electron beam on the STM measurement

When performing STM and SEM measurements simultaneously, the electron beam will temporarily hit the tunneling tip. This results in an additional current signal which can be of the same order of magnitude or larger than the tunneling current. The feedback circuit of the STM electronics cannot separate that additional signal from the tunneling current. In Fig. 6 the current resulting from the electron beam is shown. A scan of the electron beam was performed; the tip is placed in the center of the scan area. During this measurement the tip was not in tunneling contact, so all signals are a result of the electron beam only. Monitoring the current de-

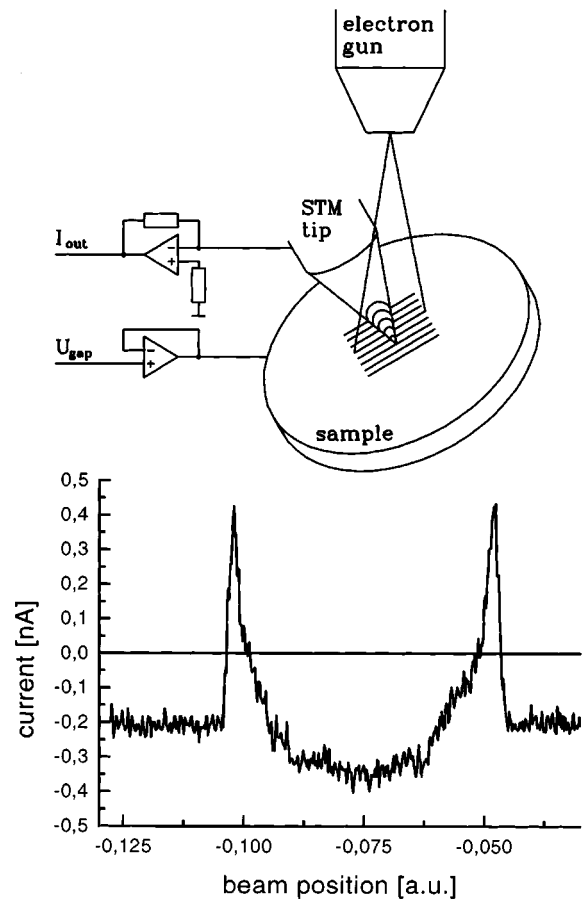


FIG. 6. Influence of the electron beam on the detected current. (Top) Schematic of the setup. U_{gap} : gap voltage. I_{out} : detected current. (Bottom) Position dependence of the detected current. The tip is placed in the center of the SEM scan. At glancing incidence a positive current is detected; the current peaks approximately mark the edges of the tip. On the sample secondary electrons are produced and detected by the tip. This current strongly depends on the selected gap voltage on the sample with respect to the tip ($+1.5$ V for the figure).

tected by the tip shows that both negative and positive net currents may result from the electron beam. The effect depends strongly on the angle of incidence between the electron beam and the tip: positive net currents (equivalent to a tunneling current from the tip to the sample) are detected at glancing incidence only, in the case of which secondary electrons are very efficiently (yield >1) produced by the electron beam. Getting closer to normal incidence the efficiency for secondary electron generation is largely reduced to less than 1 resulting in a negative net current. An electron beam current of 2 nA at 15 kV at most produces a net current of 1 nA. When the tip is not hit by the electron beam an additional signal is detected. The tunneling tip collects generated secondary electrons. This signal depends strongly on the selected gap voltage. A more positive gap voltage on the sample with respect to the tip decreases the detected current, as expected.

The interference of the electron beam on the tunneling signal will normally not result in a tip crash. Since the tunneling current rises approximately exponentially with decreasing tip-sample distance, it will compensate every signal resulting from the electron beam. Hence, to perform STM

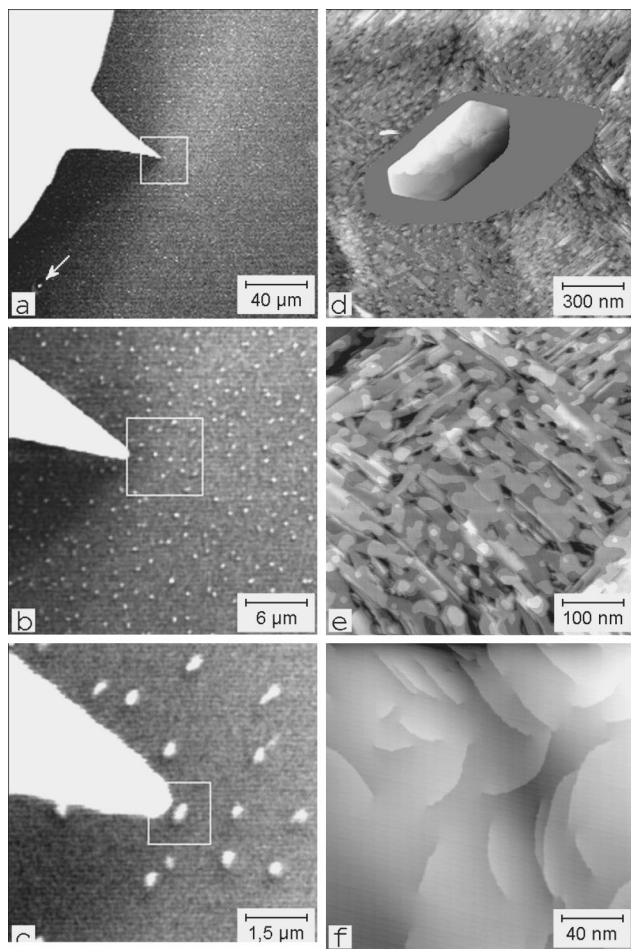


FIG. 7. Approaching a Cu microcrystallite. (a)–(c) SEM images, (d)–(f) STM images. (a) Moving the STM tip to the center of the SEM scanning area. (b) Zooming in. The microcrystallites become visible. (c) Positioning the STM tip near one microcrystallite. (d) Switching to STM, scanning the selected crystallite and its surrounding surface. For this image a double gray scale is used to show both the top of the crystallite and the surrounding surface. Regions where the gray scale is not defined are hidden. (e) Surface near the crystallite. It shows the structure of bcc Fe slabs covered with at least 1 ML of Cu. (f) Surface on top of a crystallite. A large number of screw dislocations is visible.

and SEM measurements simultaneously, the electron beam current has to be significantly smaller than the tunneling current, i.e., about a factor of 5–10. Otherwise the z resolution of the STM image is largely reduced.

D. Region recovery and tip approach

Our apparatus offers the possibility to position the STM tip on the sample under SEM control. Therefore, it is possible to retrieve a sample region repeatedly, if the sample has marks which are visible with the SEM. For example, larger crystal defects, typical shapes of the structures to be investigated or particles make convenient orientation points. By looking at such intrinsic marks with the SEM it is easily possible to accurately position the STM tip relative to the sample. An example of the region recovery procedure is given in Fig. 7.

Figure 7a shows a low magnification SEM image of the sample and the STM tip. This is a suitable magnification for coarse positioning of the STM tip, and the small dust particle

indicated by an arrow could serve as a landmark. With increased SEM magnification the characteristic pattern of smaller details of the sample surface becomes visible and allows fine adjustment of the STM position [Fig. 7(b)]. At about this magnification the automatic tip approach is started to bring the tip within a few nm of the sample surface, before doing the final positioning shown in Fig. 7(c). The accuracy of the tip approach is mainly limited by the finite radius of the tip apex. Since this is usually about a few hundred nanometers, the active region of the tip is not visible with the SEM. However, the accuracy is sufficient since the tolerance in positioning is much smaller than the maximum scan area of the scanning tunneling microscope. STM images of up to $10 \times 10 \mu\text{m}$ can be taken, this is larger than the total area shown in the SEM image [Fig. 7(c)]. The STM itself can then be used to look more closely at the sample surface. Figure 7(d) shows a medium range STM image which, besides being of interest by itself, serves to position the STM tip for the images shown in Fig. 7(e) and 7(f). This principle can be extended to even smaller image sizes, therefore a reproducible retrieval of nanometer size structures on a sample surface, for example one of the screw dislocations visible in Fig. 7(f), is possible with this combination of SEM and STM.

Figure 8 shows an example where a Cu -microcrystallite is repeatedly scanned between several annealing procedures. For annealing, the sample has been moved to the preparation chamber. Using the procedure described above, it takes only about 5 min to retrieve a specific position on the sample after reinsertion of the sample plate on the STM/SEM stage; therefore, this method allows detailed investigations of all preparation steps irrespective of whether they are situated in the analysis or the preparation chamber.

E. Auger analysis

The count rate of the Auger analyzer was checked at different beam voltages, beam currents and pass energies. For a clean copper sample we obtain for the LMM line at 920 eV an energy resolution of about 7 eV (pass energy 80 eV) and a beam current of 10 nA at 5 kV beam energy an overall count rate of about 65 kcps and a signal-to-background ratio of 1:4.8 (ratio of the intensity of the selected Auger peak with subtracted background to the intensity of the background). At 15 kV beam energy for the same energy resolution and beam current a count rate of about 23 kcps and a signal-to-background ratio of 1:2.2 are reached.

The resolution of SAM images is mainly limited by the Auger signal contribution of backscattered electrons leaving the sample remote from the primary beam spot. For a review on this topic refer to Ref. 27. To get an image showing pure material contrast the topography dependent yield of the Auger electrons has to be eliminated. This is normally done by applying background subtraction methods per line and normalization of the image to the background signal intensity. With the SAM setup a resolution of better than 100 nm is obtained. Figure 9 shows that regions of different material with a lateral size of 300–600 nm can be clearly resolved.

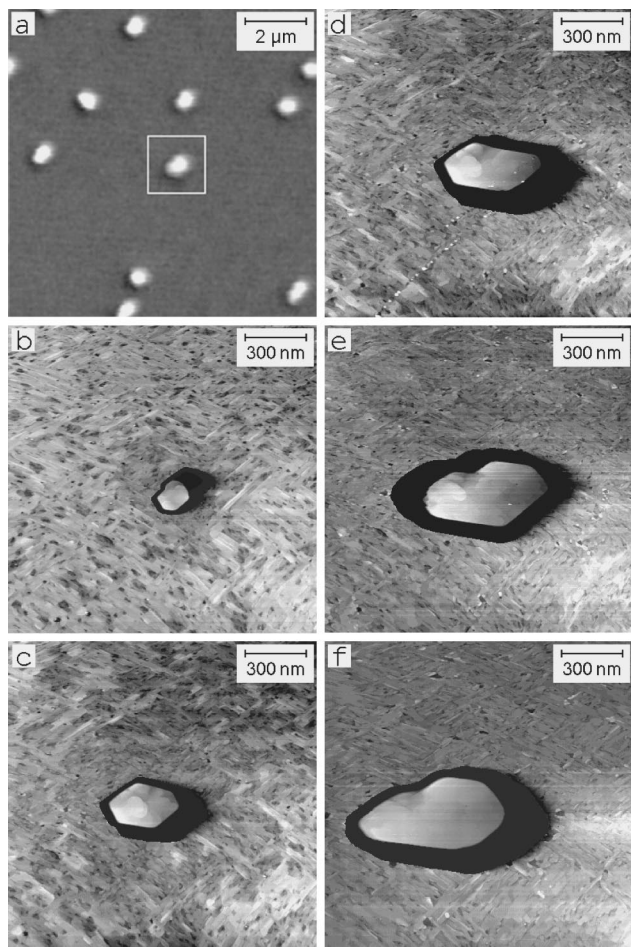


FIG. 8. Multiple scanning of a selected crystallite between several annealing cycles at 520 K. (a) SEM image of the region. The crystallite in the middle (marked with a white square) will be scanned. The image corresponds to the STM image (e). (b) STM image after 20 min annealing. (c) After additional 20 min. (d) After additional 30 min. (e) After additional 50 min. (f) After additional 180 min. The crystallite grows while the surrounding surface changes its structure; the copper overlayer disappears. Gray scales for the STM images as with Fig. 7.

IV. FIRST RESULTS

Copper microcrystallite formation takes place on a Cu/Fe/Cu(100) sample after annealing at >520 K, for a thickness of the iron layer of more than 10 ML and in the thickness range of 4–10 ML of copper. These crystallites have sizes of about 350–600 nm and heights between 25 and 70

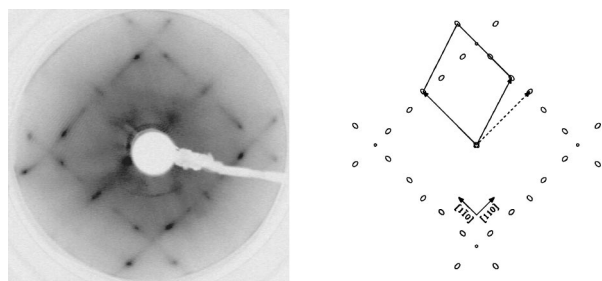


FIG. 9. (a) SAM image of several Cu microcrystallites, 650 eV iron peak. (b) SAM image, 920 eV copper peak. Due to an uncorrected image shift the images are slightly shifted against each others. (c) SEM image of the crystallites. The Auger electron spectra were taken from a crystallite and from its surrounding.

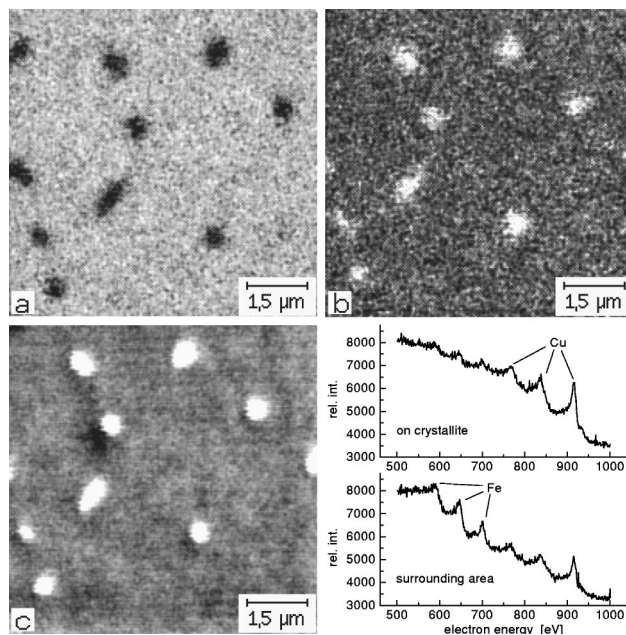


FIG. 10. (Left) LEED pattern at 157 eV of a sandwich structure of 8 ML Cu/18 ML Fe/Cu(100) after annealing for 30 min at 470 K. (Right) Schematic drawing of the observed pattern. The bcc (110) unit cell is indicated. Four different domains of iron slabs show up.

nm, depending on the thickness of the copper layer and the annealing temperature. They are separated by several microns. Therefore the probability of finding them is low. Only with a combined STM/SEM system is it possible to obtain statistical information on the crystallite size, height, and density and to get a representative overview.

As described before, Fig. 7 shows the approach to a microcrystallite, the white squares in the images mark the region of the next image. Figure 7(d) shows an STM image of a crystallite with a size of about 300–600 nm and a height of 60 nm. For convenience two gray scales are used for the figure allowing to show both the top of the crystallite and the surrounding surface. The part of the image where the gray scale is not defined is hidden. Areas on top of the crystallite [Fig. 7(f)] and of the surrounding surface [Fig. 7(e)] can be easily selected from this image.

The STM is not the appropriate tool for determining the lattice structure of the sample. Therefore LEED measurements are necessary to characterize the structure of the sandwich. In Fig. 9 (left) a LEED pattern of the sandwich structure after annealing is shown. The pattern is attributed to $\langle 110 \rangle$ bcc domains. Different domains show up, as expected from experiments described in the literature.²⁸ Figure 9 (right) gives a schematic description of the observed pattern. The pattern is equal to that of an annealed 18-ML-thick bcc Fe layer on a Cu(100) crystal, but the brightness of the spots is largely reduced.

Experiments were performed to investigate the formation mechanism of the crystallites. It is difficult to observe the growth of the crystallites with a conventional variable temperature STM^{29–31} for the following reasons: when heating the sample, it will drift with respect to the STM scanner. So the region to investigate is normally lost. Waiting for thermal stability is not possible since the formation process

is so fast that it is finished before thermal stability is reached. Measuring at lower temperatures is not useful since the sample might contaminate due to the long heating and measuring time. It is therefore necessary to let the sample cool down between the annealing cycles for performing the measurements. In this case a reproducible retrieval of a specific region is imperative. The retrieval of a region is demonstrated in Fig. 8. The upper left image shows the SEM image of the selected region, the crystallite in the center of the image is investigated. In the next images (STM measurements) of Fig. 8 several steps of the crystallite formation are shown. It can be seen that the crystallite grows and that the surrounding surface changes its structure. The crystallite height of up to 70 nm is extremely large compared with normal STM samples. Therefore double or multiple tip effects at such sharp edges can hardly be avoided. They result in shadow images of the crystallites which can be easily detected when differentiating the image. The regions of the images where multiple tip effects are present are hidden in Fig. 8. Also with these images a double gray scale is used.

Figure 10 shows Auger electron spectra and SAM images of the Cu microcrystallites. Due to small image drifts during the measurement period of time the position of the electron beam on the sample may drift. Therefore the spectrum will also include electrons from the surrounding surface. The Auger spectrum from the crystallite shows that it consists of copper. The SAM measurements, taken at 650 eV (Fe peak) and 920 eV (Cu peak), respectively, with background subtraction and normalization, show inverse images for the two energies. Several crystallites, which have sizes of about 350–650 nm are resolved.

Details of the described experiments are published elsewhere.³² Several other experiments are carried out or planned which demand the recovery of specific regions on the sample, including microstructuring, where a retrieval of the structured region is imperative.

ACKNOWLEDGMENTS

This project was supported by the Bundesministerium für Bildung, Wissenschaft, Forschung und Technologie, 13N-6124/8. A.W. thanks G.S. for the introduction on the system.

¹G. Binnig and H. Rohrer, *Helv. Phys. Acta* **55**, 726 (1982).

- ²*Scanning Tunneling Microscopy*, Springer Series on Surface Science 20, edited by H.-J. Güntherodt and R. Wiesendanger (Springer, Berlin, 1992), Vols. I and II.
- ³T. Ichinokawa, Y. Miyazaki, and Y. Koga, *Ultramicroscopy* **23**, 115 (1987).
- ⁴M. Anders, M. Mück, and C. Heiden, *Ultramicroscopy* **25**, 123 (1988).
- ⁵L. Vázquez, A. Bartholomé, R. García, A. Buendía, and A. M. Baró, *Rev. Sci. Instrum.* **59**, 1286 (1988).
- ⁶Ch. Gerber, G. Binnig, H. Fuchs, O. Marti, and H. Rohrer, *Rev. Sci. Instrum.* **57**, 221 (1986).
- ⁷R. Emch, Ph. Niedermann, P. Descouts, and O. Fischer, *J. Vac. Sci. Technol. A* **6**, 379 (1988).
- ⁸K. Takata, S. Hosoki, S. Hosaka, and T. Tajima, *Rev. Sci. Instrum.* **60**, 789 (1989).
- ⁹H. Fuchs and R. Laschinski, *Scanning* **12**, 126 (1990).
- ¹⁰H. Salemink and O. Albrechtsen, *J. Vac. Sci. Technol. B* **9**, 779 (1991).
- ¹¹E. E. Ehrlich, W. F. Smith, and A. L. de Lozanne, *J. Vac. Sci. Technol. B* **9**, 1380 (1991).
- ¹²A. O. Golubok and V. A. Timofeev, *Ultramicroscopy* **42–44**, 1558 (1992).
- ¹³M. Troyon, H. N. Lei, and A. Bourhettar, *Ultramicroscopy* **42–44**, 1564 (1992).
- ¹⁴K. Nakamoto and K. Uozumi, *Ultramicroscopy* **42–44**, 1569 (1992).
- ¹⁵G. C. Rosolen and M. E. Welland, *Rev. Sci. Instrum.* **63**, 4041 (1992).
- ¹⁶M. Takai, N. Yokoi, R. Mimura, H. Sawaragi, and R. Aihara, *Mater. Res. Soc. Symp. Proc.* **295**, 23 (1992).
- ¹⁷P. M. Thibado, Y. Liang, and D. A. Bonnell, *Rev. Sci. Instrum.* **65**, 3199 (1994).
- ¹⁸A. V. Ermakov and E. L. Garfunkel, *Rev. Sci. Instrum.* **65**, 2853 (1994).
- ¹⁹U. Memmert, U. Hodel, and U. Hartmann, *Rev. Sci. Instrum.* **67**, 2269 (1996).
- ²⁰S. Maruno, H. Nakahara, S. Fujita, H. Watanabe, Y. Kusumi, and M. Ichikawa, *Rev. Sci. Instrum.* **68**, 116 (1997).
- ²¹Raith GmbH, Hauert 18, Technologiepark, 44227 Dortmund, Germany.
- ²²FEI Company, 7425 NW Evergreen Parkway, Hillsboro, OR 97007.
- ²³This program is available from OMICRON Vakuumphysik GmbH.
- ²⁴FOCUS GmbH, Am Birkhecker Berg 20, 65510-Hünstetten-Görsroth, Germany.
- ²⁵Integrated Dynamics Engineering, Hauptstrasse 103B, 65375 Oestrich-Winkel, Germany.
- ²⁶B. S. Swartzentruber, Y. W. Mo, M. B. Webb, and M. G. Lagally, *J. Vac. Sci. Technol. A* **7**, 2901 (1989).
- ²⁷M. Prutton, *Microsc. Microanal. Microstruct.* **6**, 289 (1995).
- ²⁸W. Wuttig, B. Feldmann, J. Thomassen, F. May, H. Zillgen, A. Brodde, H. Hannemann, and H. Neddermeyer, *Surf. Sci.* **291**, 14 (1993).
- ²⁹J. W. M. Frenken, R. J. Hamers, and J. E. Demuth, *J. Vac. Sci. Technol. A* **8**, 295 (1990).
- ³⁰L. Kuipers, R. W. M. Loos, H. Neerings, J. ter Horst, G. J. Ruwiel, A. P. de Jongh, and J. W. M. Frenken, *Rev. Sci. Instrum.* **66**, 4557 (1995).
- ³¹M. Bott, T. Michely, and G. Comsa, *Rev. Sci. Instrum.* **66**, 4135 (1995).
- ³²A. Wiessner, M. Agne, D. Reuter, and J. Kirschner, *Surf. Sci.* **377–379**, 937 (1997).